






Nonlinear dynamics of the topological helicity wave in a frustrated skyrmion stringJing Xia , Xichao Zhang , and Xiaoxi Liu *Department of Electrical and Computer Engineering, Shinshu University, Wakasato 4-17-1, Nagano 380-8553, Japan*Yan Zhou *School of Science and Engineering, Chinese University of Hong Kong, Shenzhen, Guangdong 518172, China*Motohiko Ezawa *Department of Applied Physics, University of Tokyo, 7-3-1 Hongo, Tokyo 113-8656, Japan*

(Received 29 March 2022; revised 17 June 2022; accepted 29 July 2022; published 10 August 2022)

A skyrmion in a frustrated magnetic system has the helicity degree of freedom. A skyrmion string is formed in a frustrated layered system, which is well described by the XY model owing to the exchange coupling between adjacent layers. We consider a system where the interlayer exchange couplings are alternating, where the dimerized XY model is materialized, whose linear limit is the Su-Schrieffer-Heeger model. We argue that it is a nonlinear topological system. We study the quench dynamics of the helicity wave under the initial condition that the helicity of the skyrmion in the bottommost layer is rotated. It yields a good signal to detect whether the system is topological or trivial. Our results show that the helicity dynamics of the skyrmion string have a rich physics in the modulated exchange-coupled system.

DOI: [10.1103/PhysRevB.106.054414](https://doi.org/10.1103/PhysRevB.106.054414)**I. INTRODUCTION**

Both topological solitons and topological phases have been intensively studied in condensed-matter physics. The former examples are domain walls, vortices, and skyrmions, where topological numbers are defined in the coordinate space. The latter examples are topological insulators and superconductors, where topological numbers are defined in the momentum space. They are entirely different concepts and so far studied in different contexts.

Magnetic skyrmions stabilized by the Dzyaloshinskii-Moriya interaction (DMI) have been studied mainly in ferromagnets [1–4]. On the other hand, skyrmions in frustrated magnetic systems without the DMI are intriguing objects because they have the helicity degree of freedom when the magnetic dipole-dipole interaction (DDI) is weak [5–9]. The presence of the DDI leads to the Bloch-type helicity in a frustrated skyrmion [9,10]. Recently, skyrmion strings have been attracting much attention [11–13]; they are materialized in layered magnets or thick magnetic bulks.

In this work, we investigate the helicity dynamics of a skyrmion string in a layered frustrated magnetic system without the DMI, where we make the interlayer couplings alternating. An effective model is described by the XY model with dimerization. It is an intrinsically nonlinear system. The linearized limit of the dimerized XY model is the Su-Schrieffer-Heeger (SSH) model [14,15], which is the simplest example of topological insulators. Hence, we expect the helicity dynamics of a skyrmion string to share the rich topological physics with topological insulators.

To analyze the nonlinear dynamics of the helicity wave along a skyrmion string, we employ the quench dynamics, where only the helicity at the bottommost magnetic layer is rotated at the initial time. The nonlinearity is controlled by the rotation angle. When the rotation angle is small, the system is approximated by a linear model and reduced to a kind of dynamical SSH model. We find that the distinction between the topological and trivial phases remains even in the nonlinear regime. A finite standing wave is excited in the topological phase but not in the trivial phase.

This paper is composed as follows. In Sec. II, we review the helicity degrees of freedom of skyrmions in frustrated magnetic systems. In Sec. III, we study the dynamics of the helicity wave based on the linearized theory. In Sec. IV, we analyze the nonlinear helicity dynamics and find that the topological and trivial phases are well signatored by the propagation of the helicity dynamics. In Sec. V, we study the effect of disorders and show that the helicity dynamics is robust against disorders. Section VI is devoted to discussion and conclusions.

II. HELICITY DYNAMICS IN A FRUSTRATED SKYRMION STRING

A rigid nanoscale skyrmion is a centrosymmetric swirling spin texture, whose collective coordinates are the skyrmion center and the helicity η ($0 \leq \eta < 2\pi$). The spin texture located at the coordinate center is parametrized as

$$\mathbf{m}(\mathbf{r}) = (\sin \theta \cos \phi, \sin \theta \sin \phi, \cos \theta), \quad (1)$$

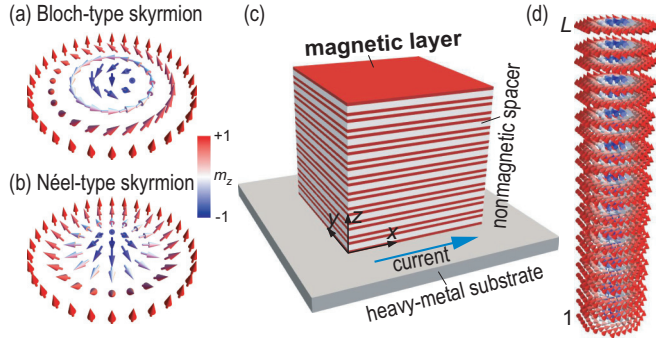


FIG. 1. (a) Schematic of a Bloch-type skyrmion. (b) Schematic of a Néel-type skyrmion. (c) Illustration of a layered frustrated magnet. The alternating thicknesses of spacers are assumed to materialize alternating interlayer exchange couplings. A heavy-metal layer is underneath the layered frustrated magnet, in which a vertical spin current could be generated to drive the helicity dynamics of the skyrmion in the bottommost magnetic layer. (d) Illustration of a 3D Bloch-type skyrmion string.

with

$$\phi = Q\varphi + \eta + \pi/2, \quad (2)$$

where φ is the azimuthal angle ($0 \leq \varphi < 2\pi$) satisfying

$$x = r \cos \varphi, \quad y = r \sin \varphi, \quad (3)$$

with $r = \sqrt{x^2 + y^2}$, and

$$Q \equiv -\frac{1}{4\pi} \int \mathbf{m}(\mathbf{r}) \cdot [\partial_x \mathbf{m}(\mathbf{r}) \times \partial_y \mathbf{m}(\mathbf{r})] d^2\mathbf{r} \quad (4)$$

is the topological number counting how many times $\mathbf{m}(\mathbf{r})$ wraps S^2 as the coordinate (x, y) spans the whole planar space. We note that there is a difference from the conventional definition in Eq. (2) by the angle $\pi/2$ because we expand the helicity around the Bloch state in order to derive the linear theory, where the Bloch state is the ground state.

Typically, there are two types of skyrmions differentiated by the helicity η . They are the Bloch-type skyrmion [Fig. 1(a)] for $\eta = 0$ and π , and the Néel-type skyrmion [Fig. 1(b)] for $\eta = \pi/2$ and $3\pi/2$ in the present convention in Eq. (2), which is different from the conventional definition by the presence of the factor $\pi/2$. The helicity η is locked in a skyrmion stabilized by the DMI in such a way that the Bloch-type [3,4] (Néel-type [16–22]) structure is realized by the bulk (interface-induced) DMI.

We first discuss a magnetic skyrmion in a frustrated monolayer, where the DMI is absent. The skyrmion energy depends on the helicity η in the presence of the magnetic DDI as [9]

$$H_{\text{DDI}} = -V \cos 2\eta, \quad (5)$$

where V is the magnitude of the potential satisfying $V > 0$. Hence, it weakly favors the Bloch-type order ($\eta = 0$ and π). In order to justify the precise shape of the energy given by Eq. (5), we calculated the DDI energy of a static skyrmion with a fixed helicity in a frustrated monolayer system without the DMI [9], where the total skyrmion energy include the ferromagnetic nearest-neighbor, antiferromagnetic next-nearest-neighbor, antiferromagnetic next-next-nearest-neighbor, DDI,

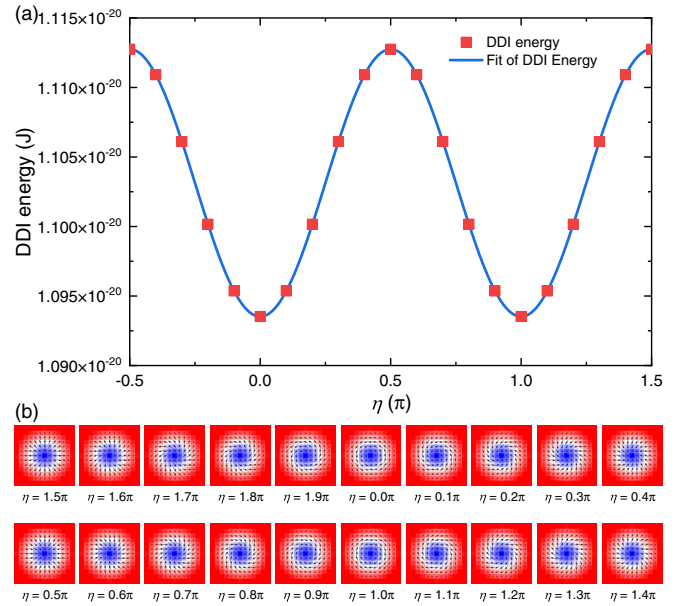


FIG. 2. (a) Simulated dipole-dipole energy of a static frustrated skyrmion as a function of the helicity η . The skyrmion energy is calculated by assuming a fixed skyrmion profile with a given helicity. The magnetic parameters are as follows: the nearest-neighbor exchange $J_1 = 30$ meV, next-nearest-neighbor exchange $J_2 = -0.8$ (in units of $J_1 = 1$), next-next-nearest-neighbor exchange $J_3 = -0.6$, and perpendicular magnetic anisotropy constant $K = 0.01$. The simulated model is a square-lattice sample of 31×31 spins with the lattice constant of 0.4 nm. More modeling details are given in Ref. [9]. Note that we do not apply an external magnetic field to stabilize the frustrated skyrmion since our system has the perpendicular magnetic anisotropy. (b) Snapshots showing the frustrated skyrmions with different η . The out-of-plane spin component is color coded: red is into the plane, blue is out of the plane, white is in-plane. The in-plane spin directions are indicated by arrows.

and perpendicular magnetic anisotropy interaction energies. The results are shown in Fig. 2. It can be seen that the skyrmion energy is well described by a cosine function, i.e., Eq. (5). We also note that the metastability phase diagram of an isolated frustrated skyrmion was reported in Ref. [9], where the minimum required value of the next-next-nearest-neighbor exchange interaction for stabilizing a skyrmion decreases with increasing magnitude of the next-nearest-neighbor and next-next-nearest-neighbor exchange interactions are antiferromagnetic exchange interactions that compete with the ferromagnetic nearest-neighbor exchange interaction.

In the present work, we consider a layered structure of frustrated skyrmions, where all magnetic layers are insulated by spacers between them, as depicted in Fig. 1(c). We focus on a skyrmion string in Fig. 1(d), where the dynamical degrees of freedom are given by the collective coordinates of each skyrmion. They are the skyrmion center and the helicity. However, it is possible to pin the center of mass of a skyrmion by fabricating a sample with an appropriate artificial pinning pattern. Indeed, this is the case in the case of ferromagnets [23].

The static skyrmion string given in Fig. 1(d) is simulated based on a frustrated multilayer system [24], where we considered 20 exchange-coupled frustrated layers. The thickness of each magnetic layer is 0.4 nm. The spacer thickness is alternating (i.e., either 0.4 nm or 0.8 nm), as shown in Fig. 1(c). The simulation parameters are the same as those used in Fig. 2 and more modeling details are given in Refs. [9,24].

III. HELICITY DEPENDENCE OF A SKYRMION

We note that Eq. (5) can be applied to all ferromagnetic layers considering the fact that the helicity of skyrmions is uniform in the thickness direction. Although the interlayer exchange coupling strengths are alternating, the skyrmion profile will be uniform in the thickness direction provided that the interlayer coupling strengths are strong enough to couple adjacent skyrmions [Fig. 1(d)]. Namely, our system is a straight skyrmion string, where the magnetic DDI energy is

$$H_{\text{DDI}} = -V \sum_{i=1}^L \cos 2\eta_i, \quad (6)$$

where i is the layer index. The interlayer coupling of the helicity between adjacent layers is described by the XY model,

$$H_{\text{inter}} = - \sum_{i=1}^L J_i (S_i^x S_{i+1}^x + S_i^y S_{i+1}^y), \quad (7)$$

because $S_i^z = 0$. By inserting Eq. (1) into this equation with $\theta = \pi/2$, we obtain

$$H_{\text{inter}} = - \sum_{i=1}^L J_i \cos(\eta_i - \eta_{i+1}). \quad (8)$$

The kinetic term is given by [25]

$$H_{\text{kine}} = m \sum_{i=1}^L \frac{1}{2} \left(\frac{d\eta_i}{dt} \right)^2, \quad (9)$$

where m is the effective mass of the helicity given by $m = J/v^2$ with v the velocity of the helicity wave along the skyrmion string for $V = 0$.

The total Hamiltonian is given by

$$H = H_{\text{kine}} + H_{\text{inter}} + H_{\text{DDI}}, \quad (10)$$

from which the equations of motion are derived,

$$m \frac{d^2 \eta_i}{dt^2} = -[J_i \sin(\eta_i - \eta_{i+1}) + J_{i-1} \sin(\eta_i - \eta_{i-1})] - 2V \sum_j \sin 2\eta_j. \quad (11)$$

We may choose the alternating interlayer coupling,

$$J_i = J(1 + \lambda(-1)^i), \quad (12)$$

or $J_i = J_A$ for even i and $J_i = J_B$ for odd i with

$$J_A = J(1 + \lambda), \quad J_B = J(1 - \lambda), \quad (13)$$

where $|\lambda| < 1$ and $J > 0$. The interlayer exchange coupling in a magnetic multilayer system depends on the thickness of the spacer due to the Ruderman-Kittel-Kasuya-Yosida (RKKY)

interaction mechanism [26–28]. Thus, the exchange coupling can be controlled by modulating the thickness of the spacer between adjacent magnetic layers. In this way, the skyrmion string is made a dimerized system.

It is convenient to introduce a new variable n so that $i = 2n - 1, 2n$ with $n = 1, 2, \dots, N/2$. The equations of motion read

$$m \frac{d^2 \eta_{2n-1}}{dt^2} = J_A \sin(\eta_{2n} - \eta_{2n-1}) + J_B \sin(\eta_{2n-2} - \eta_{2n-1}) - 2V \sin 2\eta_{2n-1}, \quad (14)$$

$$m \frac{d^2 \eta_{2n}}{dt^2} = J_B \sin(\eta_{2n+1} - \eta_{2n}) + J_A \sin(\eta_{2n-1} - \eta_{2n}) - 2V \sin 2\eta_{2n}. \quad (15)$$

We analyze the system under the initial condition,

$$\eta_n(t) = \xi \pi \delta_{n,1}, \quad \left. \frac{d\eta_i}{dt} \right|_{t=0} \quad \text{at } t = 0, \quad (16)$$

where ξ is a parameter in the range $0 \leq \xi \leq 1$. Namely, we rotate the helicity of the bottommost layer initially, and investigate how a helicity wave propagates along the skyrmion string as time evolves.

We note that the helicity of the skyrmion can be controlled by applying the dampinglike spin-orbit torque [9]. The dampinglike spin-orbit torque is directly coupled to the helicity dynamics of a frustrated skyrmion [6,9]. As shown in Fig. 1, we assume that the layered frustrated magnet is placed upon a heavy-metal substrate, which may be fabricated experimentally in a bottom-up fashion. If we apply a charge current in the heavy-metal substrate, a vertical spin current will be generated and injected into the bottommost magnetic layer due to the spin Hall effect, which only drives the rotation of the skyrmion helicity in the bottommost magnetic layer. In addition to the rotation of the helicity, the center of the skyrmion also rotates [9]. However, as we have already stated, the center-of-mass motion can be fixed by introducing the pinning center as in the case of a ferromagnet [23].

IV. LINEAR THEORY

A. SSH model

We first investigate the system where the initial helicity rotation $\xi \pi$ is tiny, $|\xi| \ll 1$, which we call the linear regime. Indeed, the equations of motion are linearized and given by

$$m \frac{d^2 \eta_i}{dt^2} = -[J_i(\eta_i - \eta_{i+1}) + J_{i-1}(\eta_i - \eta_{i-1})] - 4V \eta_i, \quad (17)$$

since we may assume $|\eta_i - \eta_{i+1}| \ll 1$ and $|\eta_i| \ll 1$. They are summarized as

$$m \frac{d^2 \eta_i}{dt^2} = \sum_j H_{ij}^{\text{Linear}} \eta_j, \quad (18)$$

where

$$H_{ij}^{\text{Linear}} = H_{ij}^{\text{SSH}} - (J_A + J_B + 4V) \delta_{ij}, \quad (19)$$

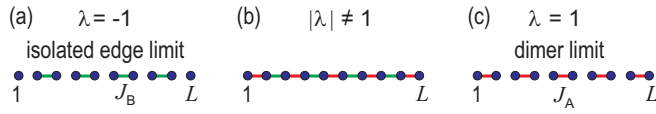


FIG. 3. Illustration of a skyrmion string, where blue disks represent skyrmions, while red and green bonds represent the couplings J_A and J_B . (a) The limit $\lambda = -1$, where the system is topological. (b) An intermediate state $|\lambda| < 1$, where it is topological or trivial. (c) The limit $\lambda = 1$, where it is trivial.

with

$$H_{ij}^{\text{SSH}} = J_A \sum_p^{L/2} (\delta_{i-j,1} \delta_{i,2p} + \delta_{j-i,1} \delta_{j,2p}) + J_B \sum_p^{L/2} (\delta_{i-j,1} \delta_{j,2p} + \delta_{j-i,1} \delta_{i,2p}). \quad (20)$$

This is the SSH model. It is expressed as

$$H^{\text{SSH}}(k) = \begin{pmatrix} 0 & J_A + J_B e^{-ik} \\ J_A + J_B e^{ik} & 0 \end{pmatrix}, \quad (21)$$

in the momentum space.

The SSH model (20) is illustrated in Fig. 3, where blue disks stand for skyrmions located in the layer i , while red and blue lines indicate the couplings J_A and J_B , respectively. There are two special limits; that is, the system has two isolated edges at $i = 1$ and L for $\lambda = -1$ as in Fig. 3(a), while all of the states are dimerized for $\lambda = 1$ as in Fig. 3(c).

B. Topological number

The SSH Hamiltonian H^{SSH} describes a topological insulator. The topological number is the Zak phase defined in the momentum space by

$$\Gamma = \frac{1}{2\pi} \int_0^{2\pi} A(k) dk, \quad (22)$$

where $A(k) = -i \langle \psi(k) | \partial_k | \psi(k) \rangle$ is the Berry connection with $\psi(k)$ the eigenfunction of $H^{\text{SSH}}(k)$. It is also the topological number of the model H^{linear} because the diagonal term in Eq. (19) does not contribute to it. We obtain $\Gamma = 1$ for $\lambda < 0$ and $\Gamma = 0$ for $\lambda > 0$. Hence, the linear system is topological for $\lambda < 0$ and trivial for $\lambda > 0$.

The topological structure of the SSH Hamiltonian H^{SSH} becomes manifest in terms of the energy spectrum in the coordinate space as a function of λ . It is shown in Fig. 4(a), where topological edge states are clearly observed at zero energy as marked in red for $-1 \leq \lambda < 0$. There are two degenerate eigenfunctions ψ^b and ψ^t localized at the bottom edge ($n = 1$) and the top edge ($n = L$) of the skyrmion string. They correspond to the two isolated disks in Fig. 3(a).

We show $|\psi^b|^2 + |\psi^t|^2$ in Fig. 4(b). It has sharp peaks at the edges $n = 1$ and L for $-1 \leq \lambda < 0$, but none for $0 \leq \lambda < 1$. The exception occurs at $\lambda = 1$, where there are peaks at $n = 1, 2, L - 1$, and L . They correspond to the two dimers at the edges in Fig. 3(c), which we discuss later; see Sec. V A. The eigenfunction $\Psi \equiv |\psi^b|^2 + |\psi^t|^2$ is plotted in Fig. 4(c), demonstrating the topological and trivial

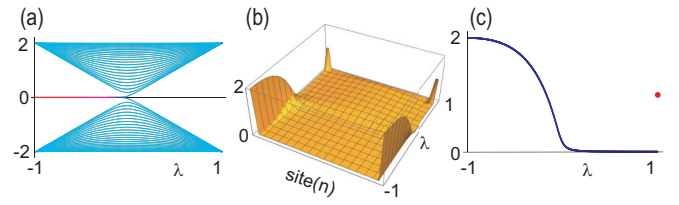


FIG. 4. (a) The energy spectrum of the SSH model as a function of λ . Topological edge states are marked in red, while the bulk states are marked in cyan. The vertical axis is energy in units of J . (b) The spatial profile of the edge states $|\psi^b|^2 + |\psi^t|^2$ as a function of λ . (c) $|\psi^b|^2 + |\psi^t|^2$ as a function of λ . Red disk at $\lambda = 1$ shows the peak amplitude owing to the dimer state. We have used a finite chain with length $L = 50$.

phases, $\Psi = 2$ at $\lambda = -1$, and it decreases monotonically and becomes $\Psi = 0$ for $0 < \lambda < 1$. Furthermore, it suddenly becomes $\Psi = 1$ at $\lambda = 1$ owing to the formation of the dimer state.

C. Helicity wave

We consider the homogeneous system with $\lambda = 0$, where the equations of motion are simply given by

$$m \frac{d^2 \eta_i}{dt^2} = J \sum_i [\eta_{i+1} + \eta_{i-1} - 2\eta_i] - 4V \eta_i. \quad (23)$$

The continuum limit reads

$$m \frac{d^2 \eta}{dt^2} = J \frac{\partial^2 \eta}{\partial x^2} - 4V \eta, \quad (24)$$

which is the wave equation. By inserting the linear wave ansatz

$$\eta = \exp[i(kx - \omega t)] \quad (25)$$

into Eq. (24), we obtain the dispersion of the helicity wave as

$$\omega = \sqrt{\frac{Jk^2 + 4V}{m}}, \quad (26)$$

which is gapped for nonzero V .

V. NONLINEAR THEORY

We proceed to analyze the system where the initial helicity rotation $\xi\pi$ is not tiny, which we call the nonlinear regime.

A. Dimer system

We have noticed the emergence of an isolated point at $\lambda = 1$ in the energy spectrum of the linear theory as in Fig. 4(c). We explore the physics of this point at $\lambda = 1$, where the system is perfectly dimerized as in Fig. 3(c). We set $V = 0$ in order to obtain analytic solution. In this case, the equations of motion are simply given by

$$m\eta_1 = -J \sin(\eta_1 - \eta_2), \quad (27)$$

$$m\eta_2 = -J \sin(\eta_2 - \eta_1), \quad (28)$$

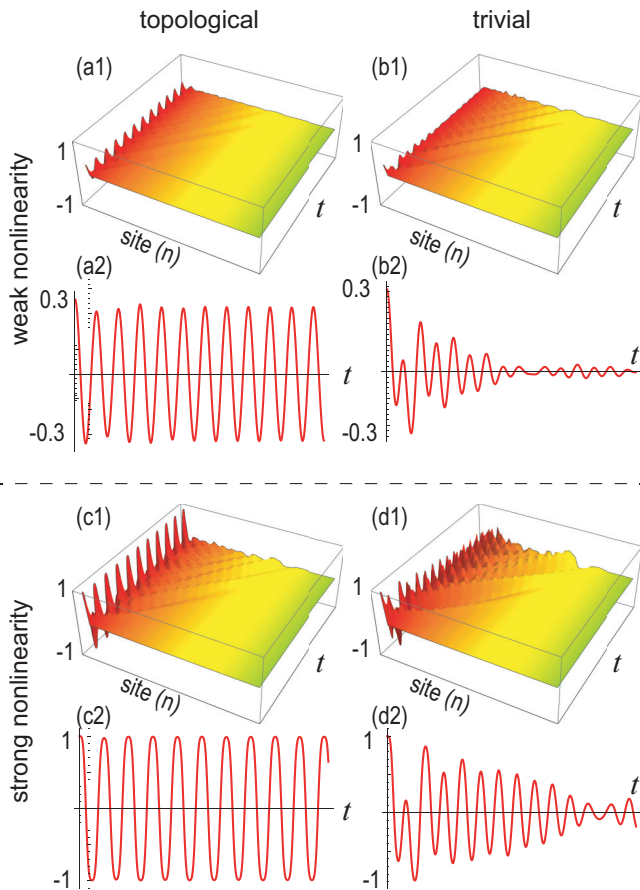


FIG. 5. Time evolution of $\sin \phi_i$ for $0 \leq t \leq 50$. (a1), (a2), (c1), and (c2) Topological phase with $\lambda = -0.5$. (b1), (b2), (d1), and (d2) Trivial with $\lambda = 0.5$. (a1), (a2), (b1), and (b2) $\xi = 0.1$. (c1), (c2), (d1), and (d2) $\xi = 0.5$. We have set $m = 1$, $J = 1$, and $V = 0.1$. We have used a finite chain with length $L = 50$.

which are equivalent to

$$m(\eta_1 + \eta_2) = 0, \quad (29)$$

$$m(\eta_1 - \eta_2) = -2J \sin(\eta_1 - \eta_2). \quad (30)$$

The solution is given by

$$\eta_1(t) = -\eta_2 + c_3 = \text{am} \left[\frac{\sqrt{(4J + c_1)(t + c_2)^2}}{2}, \frac{8J}{4J + c_1} \right], \quad (31)$$

where c_1 , c_2 , and c_3 are determined from the initial condition, or by solving $\eta_1(0) = \xi\pi$, and “am” represents the Jacobi amplitude function. This solution indicates that there is an oscillation in the two layers at the bottom edge at $\lambda = 1$, and hence we call it a dimer state. Numerical analysis shows the emergence of the dimer state also at $\lambda \neq 1$, forming a dimer phase in the nonlinear regime, as we will discuss.

B. Quench dynamics of a helicity wave

We analyze the quench dynamics of the system under the initial condition (16) numerically for $-1 \leq \lambda \leq 1$ and for $0 \leq \xi \leq 1$. The time evolution of $\sin \eta_i$ is shown in Fig. 5. There is

a finite stationary oscillation at the site $i = 1$ in the topological phase as shown in Fig. 5(a2), but this is not the case in the trivial phase as shown in Fig. 5(b2). This feature holds also for the case with $\xi = 0.5$ as shown in Figs. 5(c2) and 5(d2).

Figure 5 indicates that the amplitude after long enough time is a good signal to detect whether the system is topological or trivial. To detect it quantitatively, we define an indicator with the use of the maximum value of $\sin |\eta_1|$ as

$$\Phi(\lambda, \xi) = \max_{0.9T < t < T} [\sin |\eta_1|], \quad (32)$$

taking large enough T so that the time evolution of η_1 becomes stationary. We show $\Phi(\lambda, \xi)$ for $-1 \leq \lambda \leq 1$ by taking typical values of ξ in Fig. 6. In the weak nonlinear regime, Φ is finite in the topological phase while it is almost zero in the trivial phase, as shown in Fig. 6(a). As the increase of the nonlinearity ($\xi \rightarrow 1$), the finite region of Φ is expanded in the vicinity of $\lambda = 1$, forming the dimer phase, as shown in Figs. 6(b)–6(d).

There is only a slight difference in the indicator Φ for various V in the topological phase as shown in Fig. 6. On the other hand, the peak value of Φ is identical between $\lambda = 1$ and $\lambda = -1$ due to the energy conservation.

C. Phase diagram

The indicator Φ is shown in the λ - ξ plane in Fig. 7. We find three phases: the topological, trivial, and dimer phases. In the isolated limit $\lambda = -1$, $\Phi = \sin \xi\pi$ for $\xi \leq 1/2$ and $\Phi = 1$ for $1/2 \leq \xi \leq 1$. The topological distinction is hard to see for $\xi \simeq 0$ because $\sin \xi\pi$ is very small. However, there is a clear distinction between the topological and trivial phase as shown in Fig. 6(a). The phase boundary between the topological and trivial phase is always $\lambda = 0$ even in the nonlinear regime. On the other hand, the dimer phase emerges in the trivial phase when the nonlinearity exists. The region of the dimer phase consists of a point at $\xi = 0$ but occupies a quite large area for $\xi \gtrsim 1/2$.

A comment is in order with respect to the color difference between Figs. 7(a) and 7(c) especially in the vicinities of $\lambda = 0$ and $\xi = 0$ in the topological phase. We have used the color palette (b) to make (a), where the excitation of the helicity wave is very small in these region although they belong to the topological phase. This is clearly seen in Fig. 6.

VI. DISORDER EFFECTS

We next analyze the effect of the randomness in the exchange interaction. It is naturally introduced by the randomness in the thickness of the spacer layers. We introduce randomness by $J_A \rightarrow J_A(1 + \zeta)$ and $J_B \rightarrow J_B(1 + \zeta)$, where ζ is a uniformly distributed random real number satisfying $|\zeta| < R$.

We show the phase indicator for various randomness R in Fig. 8. The effect of the randomness is small for the topological and dimer phases. On the other hand, the trivial phase is largely affected. Namely, the propagation of the helicity wave is suppressed by the presence of the disorder. In order to observe a sharp topological phase transition, we need to use a sample with $R < 0.1$.

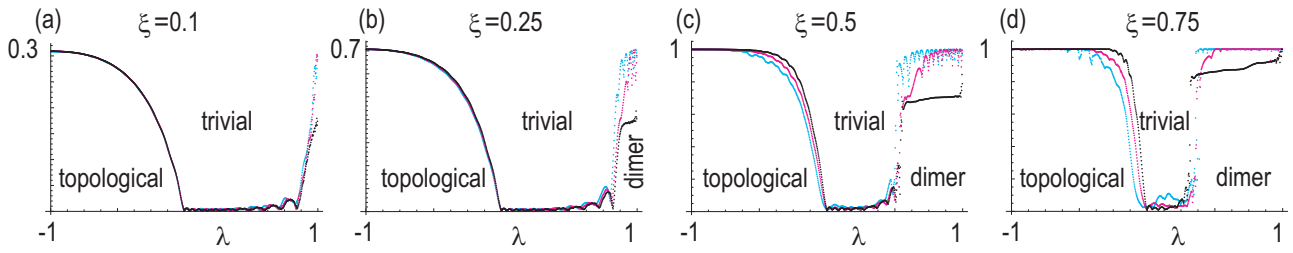


FIG. 6. Phase indicator Φ as a function of the dimerization λ . (a) $\xi = 0.1$, (b) $\xi = 0.25$, (c) $\xi = 0.5$, and (d) $\xi = 0.75$. Black curves indicate $V = 0$, magenta curves indicate $V = 0.1$, and cyan curves indicate $V = 0.2$. We have set $m = 1$, $J = 1$, $L = 50$, and $T = 100$.

A comment is in order with respect to the uniformly distributed random real number for simulations. We have employed it because the requirement that the quality is R in the quality management means that the deviation is smaller than R at most. For example, if $R = 0.1$, there should be no sample exceeding $R = 0.1$. It is naturally described by the uniformly distributed random number. On the contrary, in the case of the normal distributed random number, there is a possibility that the deviation exceeds R even if its probability is very small, which is unacceptable in the quality management.

In experiments, the interlayer exchange interaction is subject to the thicknesses of both the magnetic layer and the nonmagnetic spacer according to the RKKY-type exchange interaction mechanism. For example, the RKKY coupling field (i.e., the interlayer exchange coupling) was measured as functions of the thicknesses of Ru, Co, and Pt layers for synthetic antiferromagnetic Pt/Co/Ru multilayers [29]. The 10% deviation of the exchange interaction corresponds to the thickness deviation of the Ru layer, which is about 0.015 nm.

VII. DISCUSSION AND CONCLUSION

In this work, we have explored the nonlinear helicity dynamics of a skyrmion string in a layered frustrated magnet, where the interlayer coupling is alternating. The topological physics of the SSH model well survives although the governing equation is a nonlinear model. Our results show that an introduction of the interlayer degree of freedom may give us a rich physics in the dynamics of a skyrmion string.

To analyze the nonlinear topological dynamics, we employed the method of the quench dynamics under the initial

condition with only the edge site being excited to differentiate the topological and trivial phases [30–32]. The method has been already applied to nonlinear systems including photonic [33–36], mechanical [32,37,38], and electric circuit [30,39] systems. The present work shows that it is also applicable to magnetic systems.

There are some reports on topological phases in magnetic systems with low-energy magnon excitations [40–44]. Spin-wave dynamics has been studied in dimerized spin-torque oscillator arrays by using the Holstein-Primakoff transformation [45]. It simulates the SSH model in magnetic systems, where the bonding is dimerized. The SSH model is a typical model of a topological insulator. Nonlinear dynamics of the non-Hermitian SSH model has also been studied in the same system [46].

We note that we only focused on the skyrmion string dynamics at zero temperature in this work. The effect of temperature on a skyrmion string could be very complicated. In theory, the stability and the lifetime of a skyrmion string depend on the temperature. The thermal effect may result in the collapse of a skyrmion string. Besides, a skyrmion will show the Brownian motion at finite temperatures [47]. It is expected that a skyrmion string will also show the Brownian motion at finite temperatures, where the skyrmion string diffusion increases with increasing temperature. These dynamic effects induced by temperature will complicate the helicity dynamics of a skyrmion string.

On the other hand, we point out that our simulation result given in Fig. 1(d) suggests that the two-dimensional skyrmion profiles do not shift with respect to each other in the thickness dimension. The reason could be that the size of the frustrated skyrmion is so small that the DDI does not induce the inhomogeneity in the skyrmion structure in the thickness dimension. However, one should note that a skyrmion string made of larger ferromagnetic skyrmions or skyrmion bubbles in chiral magnets may show a wiggling structure along the z direction [48–51], which is not significant in our system.

It is worth mentioning that the propagation dynamics of spin excitations along skyrmion strings have been directly evaluated in a recent experimental report [52], which is realized by measuring the magnetic contribution to the complex spectra of self-inductance and mutual inductance for coplanar waveguides. Also, the dynamics of a 3D skyrmion string can be experimentally imaged by using a scalar magnetic x-ray tomography measurement system [50]. In principle, these experimental techniques can be employed to observe and measure the helicity wave excitation of a skyrmion string.

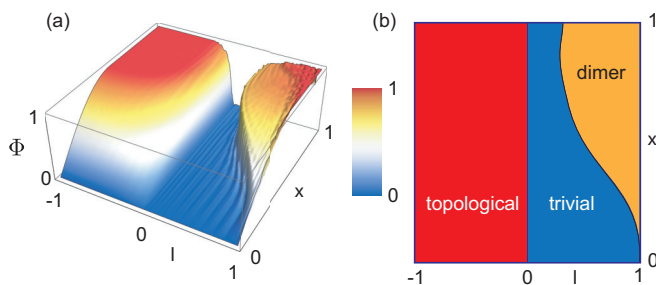


FIG. 7. Phase indicator Φ in the λ - ξ plane. (a) Bird's eye view together with the color palette indicating the amplitude. We have set $V = 0.2$, $m = 1$, $J = 1$, $L = 50$, and $T = 100$. (b) Schematic illustration of the phase diagram.

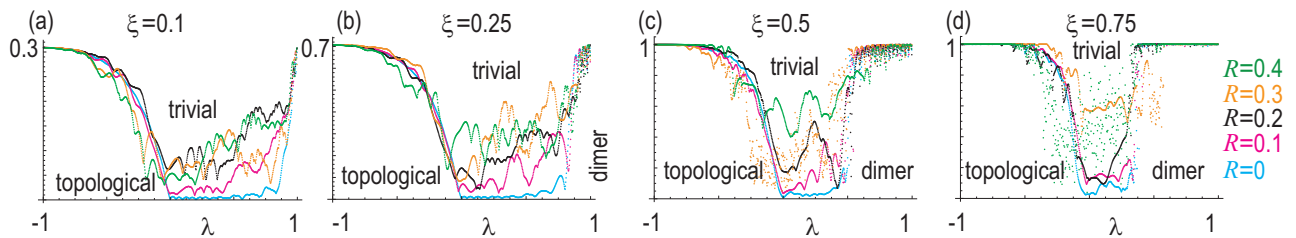


FIG. 8. Disorder effects of the phase indicator Φ as a function of the dimerization λ . (a) $\xi = 0.1$, (b) $\xi = 0.25$, (c) $\xi = 0.5$, and (d) $\xi = 0.75$. Cyan curves indicate $R = 0$, magenta curves indicate $R = 0.1$, orange curves indicate $R = 0.2$, red curves indicate $R = 0.3$, and green curves indicate $R = 0.4$. We have set $m = 1$, $J = 1$, $V = 0.2$, $L = 50$, and $T = 100$.

It would be interesting if we could use a skyrmion string as an information transmission channel, where the information is carried by the helicity wave.

ACKNOWLEDGMENTS

M.E. is very grateful to N. Nagaosa for helpful discussions on the subject. This work is supported by Grants-in-Aid for Scientific Research from MEXT KAKENHI (Grants No. JP17K05490 and No. JP18H03676). This work is also supported by CREST, JST (Grants No. JPMJCR16F1 and No. JPMJCR20T2). J.X. was an International Research Fellow of the Japan Society for the Promotion of Science (JSPS). J.X.

was supported by JSPS KAKENHI (Grant No. JP22F22061). X.L. acknowledges support by Grants-in-Aid for Scientific Research from JSPS KAKENHI (Grants No. JP21H01364, No. JP21K18872, and No. JP22F22061). Y.Z. acknowledges support by Guangdong Basic and Applied Basic Research Foundation (Grant No. 2021B1515120047), Guangdong Special Support Project (Grant No. 2019BT02X030), Shenzhen Fundamental Research Fund (Grant No. JCYJ20210324120213037), Shenzhen Peacock Group Plan (Grant No. KQTD20180413181702403), Pearl River Recruitment Program of Talents (Grant No. 2017GC010293), and National Natural Science Foundation of China (Grants No. 11974298, No. 12004320, and No. 61961136006).

- [1] A. N. Bogdanov and D. A. Yablonskii, *Sov. Phys. JETP* **68**, 101 (1989).
- [2] U. K. Rößler, A. N. Bogdanov, and C. Pfleiderer, *Nature (London)* **442**, 797 (2006).
- [3] S. Mühlbauer, B. Binz, F. Jonietz, C. Pfleiderer, A. Rosch, A. Neubauer, R. Georgii, and P. Böni, *Science* **323**, 915 (2009).
- [4] X. Z. Yu, Y. Onose, N. Kanazawa, J. H. Park, J. H. Han, Y. Matsui, N. Nagaosa, and Y. Tokura, *Nature (London)* **465**, 901 (2010).
- [5] A. O. Leonov and M. Mostovoy, *Nat. Commun.* **6**, 8275 (2015).
- [6] S.-Z. Lin and S. Hayami, *Phys. Rev. B* **93**, 064430 (2016).
- [7] C. D. Batista, S.-Z. Lin, S. Hayami, and Y. Kamiya, *Rep. Prog. Phys.* **79**, 084504 (2016).
- [8] H. T. Diep, *Entropy* **21**, 175 (2019).
- [9] X. Zhang, J. Xia, Y. Zhou, X. Liu, H. Zhang, and M. Ezawa, *Nat. Commun.* **8**, 1717 (2017).
- [10] T. Kurumaji, T. Nakajima, M. Hirschberger, A. Kikkawa, Y. Yamasaki, H. Sagayama, H. Nakao, Y. Taguchi, T.-H. Arima, and Y. Tokura, *Science* **365**, 914 (2019).
- [11] P. Sutcliffe, *Phys. Rev. Lett.* **118**, 247203 (2017).
- [12] F. Kagawa, H. Oike, W. Koshibae, A. Kikkawa, Y. Okamura, Y. Taguchi, N. Nagaosa, and Y. Tokura, *Nat. Commun.* **8**, 1332 (2017).
- [13] T. Yokouchi, S. Hoshino, N. Kanazawa, A. Kikkawa, D. Morikawa, K. Shibata, T. Arima, Y. Taguchi, F. Kagawa, N. Nagaosa, and Y. Tokura, *Sci. Adv.* **4**, eaat1115 (2018).
- [14] W. P. Su, J. R. Schrieffer, and A. J. Heeger, *Phys. Rev. Lett.* **42**, 1698 (1979).
- [15] A. J. Heeger, S. Kivelson, J. R. Schrieffer, and W.-P. Su, *Rev. Mod. Phys.* **60**, 781 (1988).
- [16] W. Jiang, P. Upadhyaya, W. Zhang, G. Yu, M. B. Jungfleisch, F. Y. Fradin, J. E. Pearson, Y. Tserkovnyak, K. L. Wang, O. Heinonen, S. G. E. te Velthuis, and A. Hoffmann, *Science* **349**, 283 (2015).
- [17] S. Woo, K. Litzius, B. Krüger, M.-Y. Im, L. Caretta, K. Richter, M. Mann, A. Krone, R. M. Reeve, M. Weigand, P. Agrawal, I. Lemesch, M.-A. Mawass, P. Fischer, M. Kläui, and G. S. D. Beach, *Nat. Mater.* **15**, 501 (2016).
- [18] C. Moreau-Luchaire, C. Moutafis, N. Reyren, J. Sampaio, C. A. F. Vaz, N. Van Horne, K. Bouzehouane, K. Garcia, C. Deranlot, P. Warnicke, P. Wohlhüter, J. M. George, M. Weigand, J. Raabe, V. Cros, and A. Fert, *Nat. Nanotechnol.* **11**, 444 (2016).
- [19] O. Boule, J. Vogel, H. Yang, S. Pizzini, D. de Souza Chaves, A. Locatelli, T. Onur Mentes, A. Sala, L. D. Buda-Prejbeanu, O. Klein, M. Belmeguenai, Y. Roussigné, A. Stashkevich, S. M. Chérif, L. Aballe, M. Foerster, M. Chshiev, S. Auffret, I. M. Miron, and G. Gaudin, *Nat. Nanotechnol.* **11**, 449 (2016).
- [20] A. Soumyanarayanan, M. Raju, A. L. Gonzalez Oyarce, A. K. C. Tan, M.-Y. Im, A. P. Petrović, P. Ho, K. H. Khoo, M. Tran, C. K. Gan, F. Ernult, and C. Panagopoulos, *Nat. Mater.* **16**, 898 (2017).
- [21] W. Jiang, X. Zhang, G. Yu, W. Zhang, X. Wang, M. Benjamin Jungfleisch, J. E. Pearson, X. Cheng, O. Heinonen, K. L. Wang, Y. Zhou, A. Hoffmann, and S. G. E. Velthuis, *Nat. Phys.* **13**, 162 (2017).
- [22] K. Litzius, I. Lemesch, B. Krüger, P. Bassirian, L. Caretta, K. Richter, F. Buttner, K. Sato, O. A. Tretiakov, J. Forster, R. M. Reeve, M. Weigand, I. Bykova, H. Stoll, G. Schutz, G. S. D. Beach, and M. Kläui, *Nat. Phys.* **13**, 170 (2017).

- [23] X. Zhang, J. Xia, K. Shirai, H. Fujiwara, O. A. Tretiakov, M. Ezawa, Y. Zhou, and X. Liu, *Commun. Phys.* **4**, 255 (2021).
- [24] X. Zhang, J. Xia, O. A. Tretiakov, H. T. Diep, G. Zhao, J. Yang, Y. Zhou, M. Ezawa, and X. Liu, *Phys. Rev. B* **104**, L220406 (2021).
- [25] X. Leoncini, A. D. Verga, and S. Ruffo, *Phys. Rev. E* **57**, 6377 (1998).
- [26] M. A. Ruderman and C. Kittel, *Phys. Rev.* **96**, 99 (1954).
- [27] T. Kasuya, *Prog. Theor. Phys.* **16**, 45 (1956).
- [28] K. Yosida, *Phys. Rev.* **106**, 893 (1957).
- [29] W. Legrand, D. Maccariello, F. Ajejas, S. Collin, A. Vecchiola, K. Bouzehouane, N. Reyren, V. Cros, and A. Fert, *Nat. Mater.* **19**, 34 (2020).
- [30] M. Ezawa, *J. Phys. Soc. Jpn.* **91**, 024703 (2022).
- [31] M. Ezawa, *Phys. Rev. B* **104**, 235420 (2021).
- [32] M. Ezawa, *J. Phys. Soc. Jpn.* **90**, 114605 (2021).
- [33] D. Leykam and Y. D. Chong, *Phys. Rev. Lett.* **117**, 143901 (2016).
- [34] X. Zhou, Y. Wang, D. Leykam, and Y. D. Chong, *New J. Phys.* **19**, 095002 (2017).
- [35] L. J. Maczewsky, M. Heinrich, M. Kremer, S. K. Ivanov, M. Ehrhardt, F. Martinez, Y. V. Kartashov, V. V. Konotop, L. Torner, D. Bauer, and A. Szameit, *Science* **370**, 701 (2020).
- [36] Y. Hadad, A. B. Khanikaev, and A. Alu, *Phys. Rev. B* **93**, 155112 (2016).
- [37] D. D. J. M. Snee and Y.-P. Ma, *Extreme Mech. Lett.* **30**, 100487 (2019).
- [38] P.-W. Lo, C. D. Santangelo, Bryan Gin-ge Chen, C.-M. Jian, K. Roychowdhury, and M. J. Lawler, *Phys. Rev. Lett.* **127**, 076802 (2021).
- [39] Y. Hadad, J. C. Soric, A. B. Khanikaev, and A. Alù, *Nat. Electron.* **1**, 178 (2018).
- [40] R. Shindou, R. Matsumoto, S. Murakami, and J. I. Ohe, *Phys. Rev. B* **87**, 174427 (2013).
- [41] R. Chisnell, J. S. Helton, D. E. Freedman, D. K. Singh, R. I. Bewley, D. G. Nocera, and Y. S. Lee, *Phys. Rev. Lett.* **115**, 147201 (2015).
- [42] S. K. Kim, H. Ochoa, R. Zarzuela, and Y. Tserkovnyak, *Phys. Rev. Lett.* **117**, 227201 (2016).
- [43] A. Rückriegel, A. Brataas, and R. A. Duine, *Phys. Rev. B* **97**, 081106(R) (2018).
- [44] L. Chen, J.-H. Chung, B. Gao, T. Chen, M. B. Stone, A. I. Kolesnikov, Q. Huang, and P. Dai, *Phys. Rev. X* **8**, 041028 (2018).
- [45] B. Flebus, R. A. Duine, and H. M. Hurst, *Phys. Rev. B* **102**, 180408(R) (2020).
- [46] P. M. Gunnink, B. Flebus, H. M. Hurst, and R. A. Duine, *Phys. Rev. B* **105**, 104433 (2022).
- [47] L. Zhao, Z. Wang, X. Zhang, X. Liang, J. Xia, K. Wu, H.-A. Zhou, Y. Dong, G. Yu, K. L. Wang, X. Liu, Y. Zhou, and W. Jiang, *Phys. Rev. Lett.* **125**, 027206 (2020).
- [48] H. R. O. Sohn, S. M. Vlasov, V. M. Uzdin, A. O. Leonov, and I. I. Smalyukh, *Phys. Rev. B* **100**, 104401 (2019).
- [49] M. T. Birch, D. Cortés-Ortuño, L. A. Turnbull, M. N. Wilson, F. Groß, N. Träger, A. Laurenson, N. Bukin, S. H. Moody, M. Weigand, G. Schütz, H. Popescu, R. Fan, P. Steadman, J. A. T. Verezhak, G. Balakrishnan, J. C. Loudon, A. C. Twitchett-Harrison, O. Hovorka, H. Fangohr, F. Y. Ogrin, J. Gräfe, and P. D. Hatton, *Nat. Commun.* **11**, 1726 (2020).
- [50] S. Seki, M. Suzuki, M. Ishibashi, R. Takagi, N. D. Khanh, Y. Shiota, K. Shibata, W. Koshibae, Y. Tokura, and T. Ono, *Nat. Mater.* **21**, 181 (2022).
- [51] A. O. Leonov, C. Pappas, and I. I. Smalyukh, *Phys. Rev. B* **104**, 064432 (2021).
- [52] S. Seki, M. Garst, J. Waizner, R. Takagi, N. D. Khanh, Y. Okamura, K. Kondou, F. Kagawa, Y. Otani, and Y. Tokura, *Nat. Commun.* **11**, 256 (2020).